Interaction of Air Motion with the Human Body

Jay B. Myers
Student Member ASHRAE

Mohammad H. Hosni, Ph.D.
Member ASHRAE

Byron W. Jones, Ph.D., P.E.
Member ASHRAE

ABSTRACT

Proper distribution of conditioned air plays a major role in both human thermal comfort and indoor air quality. The objectives of this study were (1) to experimentally evaluate airflow conditions around the human body and (2) to characterize the interaction of the thermal plume from the body with the overall room air motion. Environmental conditions around a simulated human body were examined by mapping temperature and velocity distributions around a thermal manikin using modern temperature and velocity instrumentation in an environmental chamber. Results are presented for three test cases: baseline velocity and temperature distribution without manikin, airflow blockage of the unheated manikin, and mixed convection due to interaction of chamber airflow with the heated manikin.

Air movement data collected near the thermal manikin demonstrate both the blockage effect of and thermal plumes from the thermal manikin. The unheated thermal manikin exhibited a localized blockage effect to a distance of 0.15 m (6 in.) behind the manikin. The velocity and temperature boundary layer of the thermal manikin expanded further from the body in the mixed convection case than in the unheated blockage case. Near the manikin skin surface, the velocity distribution for mixed convection was primarily dependent on the room air motion and the blockage effect of the manikin and was independent of natural convective effects. The temperature boundary layer was substantially influenced by natural convection below chest level, while at and above chest level, the temperature distribution was affected by room air motion, the blockage effect, and the heating of the manikin. The total power to the heated thermal manikin was set at 164 W (561 Btu/h), to represent a person with a modest activity level (1.5 met). The distribution of the heat loss over the surface of the manikin was determined by the manikin's heaters and, to a reasonable approximation, represents the heat distribution of a person.

INTRODUCTION

Total environmental quality, as described by Int-Hout (1993) is the concept that the environmental factors of thermal comfort, acoustics, indoor air quality, and air distribution all are interrelated. Room conditions should be controlled for comfortable temperature and air velocity, with enough fresh air at a proper flow rate for contaminant removal, and at an acceptably low noise level. Proper temperature and velocity distributions in the occupied zone are good indicators of thermal comfort. Good air distribution and thermal comfort may be achieved through proper air mixing and by avoiding drafts caused by excessive thermal gradients, high air velocity, or high air turbulence. Previous studies investigated the flow conditions near the body using human subjects, heated models, and unheated manikins; however, these studies determined the heat transfer from the body and the airflow characteristics around the body separately without specifically addressing the integration of the thermal plume from the body with the room air motion.

Thermal comfort and room air movement research began at the ASHVE /U. S. Bureau of Mines laboratory in Pittsburgh, which was founded in 1919. Houghten and Yagloglou (1923a) used human subjects in 440 comfort experiments in still air to determine conditions of equal comfort independent of humidity. Next, Houghten and Yagloglou (1923b) tested various still air conditions with 130 human subjects to find a comfort zone on the psychometric chart. The subjects rated the environment on a scale from 1 to 5. The comfort zone was bounded by conditions that 50% or more of the subjects rated as comfortable, with a rating of 2 to 4. In 1924, Houghten and Yagloglou contrasted still air conditions with the cooling effects of air movement at elevated temperatures with velocities up to 2.5 m/s (500 fpm). In later research, Houghten, Gutberlet, and Witkowski (1938) examined the effect of drafts on the backs of necks and ankles in human subjects.

Jay B. Myers is a test engineer with the Boeing Company, Wichita, Kans. **Mohammad H. Hosni** is director, Institute for Environmental Research, and **Byron W. Jones** is head of the Department of Mechanical Engineering, Kansas State University, Manhattan.

They found that thermal plumes from free convection were sufficient to mix carbon dioxide and moisture from room occupants into room air. They also observed the relationship between skin temperature at the neck or ankle and the sensation of coolness or comfort observed by the subject. The authors observed a correlation between the drop in skin temperature of the neck or ankle and the temperature and velocity of the air directed on those body parts. Data on these relationships were presented along with comfort sensations of the subjects. The most commonly used comfort index of that era varied from one to seven. A draft chart was prepared showing the relationship between the temperature and velocity of a draft and the skin temperature of the neck. The term "draft" denotes a movement of air. As defined in *ANSI/ASHRAE Standard 55-1992*, draft is the unwanted local cooling of the body caused by air movement. It is a common cause of discomfort. Draft was concluded to be caused either by high air velocity, low air temperature, excessive radiation to a cold surface, or any combination of these three effects.

In addition to air temperature, air velocity, and radiation effects, the role of velocity fluctuations on the sensation of draft has been investigated. Fanger and Pedersen (1977) exposed subjects to well-defined periodic velocity fluctuations in a climate chamber and showed that periodically fluctuating airflow is more uncomfortable than nonfluctuating airflow. Subsequent studies have supported the idea that air turbulence is a contributing factor to discomfort (Fanger et al. 1988).

An important factor in environmental quality is proper room air distribution. Most studies of air distribution have concentrated on the ability of inlets, diffusers, and other air movement equipment to distribute air through the room. Recent studies have combined this interest with examining turbulence and other statistical information related to velocity measurements. Indices of thermal comfort and air distribution have also been developed to measure and predict environmental quality. Thermal comfort has been characterized by the predicted mean vote (PMV) and predicted percentage dissatisfied (PPD) (Fanger 1973). Air distribution quality was evaluated through the introduction of the air diffusion performance index (ADPI) (Miller and Nash 1971). These indoor climate evaluation methods were developed and refined by many studies of actual comfort and room condition measurements; they have a strong statistical basis, as well as general acceptance.

The air velocities in the boundary layer surrounding the human body and within the thermal plume above the body were found to be comparable to those in the occupied zone of a typical room. While both natural convection from the body and forced convection from room air motion affect the airflow characteristics near the body, understanding the interactions of both heat transfer mechanisms is important in evaluating local airflow and thermal characteristics at the skin surface of a human body and its effects on thermal comfort.

Lewis et al. (1969) examined the boundary layer and thermal plumes associated with the human body. Their focus was to study the relationship between the boundary layers and the movement of contaminants around the human body. The expansion of the boundary layer was described, and air velocities were measured around several body segments.

Rapp (1973) analyzed an approximate model of a human body using a sphere on a cylinder to determine the convective heat transfer coefficient for humans and the relative effect of free and forced convection at low velocity airflow. He concluded that when room air speed exceeds about 0.2 m/s (39.4 fpm), forced convection conditions prevail as free convection is assumed comparatively negligible. In the velocity range between 0.01 and 0.2 m/s (2 and 39.4 fpm), convection was influenced by both free convection and room air movement and the mixed convection conditions were present.

Homma and Yakiyama (1988) employed human subjects and a heated rectangular human-sized manikin to study free convection around the human body. The authors concluded that the flow became turbulent at about the hip level, that the free convection was equal in velocity to acceptable upper limits for comfort, and that natural convection may affect room air mixing.

Chang and Gonzalez (1991) measured airflow patterns in an environmental chamber with a standing unheated manikin and its supporting frame as flow obstructions. The manikin caused decreased velocities both in front and behind it, but above the manikin head, little variance was observed. Chang and Gonzalez (1993) measured air velocities around an unheated standing or sitting manikin as an obstruction. Velocities were measured by six omnidirectional thermal anemometers mounted on a telescoping tripod support. Velocities were measured at eight radial positions (45° spacing) around the manikin's head, chest, upper arm, lower arm, thigh, and lower leg. The authors concluded that the complex and asymmetrical velocity profiles around the human body could only be measured by multiple anemometers or multiple position mapping.

Hosni et al. (1994) obtained room air motion data in a full-size test room using three different diffusers for both isothermal and nonisothermal conditions. Jet throw, drop, and spread were examined through flow visualization and velocity and temperature mapping. The blockage and deflection of airflow around obstructions were observed for both isothermal and nonisothermal conditions.

Brohus and Nielsen (1994) used a thermal manikin with an artificial lung for simulation of breathing in a full-scale test room to evaluate contaminant distribution around persons in rooms ventilated by displacement ventilation. The measurements were performed in three full-scale test rooms with different wall-mounted low-velocity inlet devices. A point heat source, a heated cylinder, and a thermal manikin were used as heat sources. A thermal and a passive contaminant source were used and the vertical concentration profiles were obtained. The stratification effect in the displacement venti-

lated room was observed from the concentration profiles. Personal exposure to contaminants was evaluated for a sitting and a standing person. It was concluded that when the movement of people around the room or the disturbance in the room increases, the ventilation effectiveness decreases and the risk of exposure to contaminants increases. The authors also found that the thermal boundary layer along a person's height is able to entrain air from below the breathing zone. If the concentration of the contaminants at the breathing level is high, this entrainment of fresher air from below enhances air quality; however, if the concentration is higher at the lower level than in the breathing zone, this entrainment may increase the risk of contaminant exposure.

Numerical modeling of room air motion and numerical simulation of airflow around a heated manikin have gained momentum in recent years due to the availability of computers and a large increase in their computational power. Murakami and Kato (1989) and Murakami et al. (1988) applied numerical methods using the k-ε turbulence model to simulate the velocity and diffusion patterns in a conventional clean room using scale models, as well as for evaluation of air distribution in a room. Since this paper deals with experimental measurements, numerical modeling results are not presented.

The objectives of this research project were (1) to experimentally measure the temperature and velocity distributions around the human body and (2) to characterize the interaction of the thermal plume from the body with the overall room air motion. A thermal manikin was used to simulate the human body, and the environmental conditions around the body were investigated using modern temperature and velocity sensors. The thermal manikin was controlled to generate a surface temperature distribution consistent with the skin temperatures of a typical person. The primary advantage of using the thermal manikin over human subjects was the repeatable control of skin temperatures for extended periods. The thermal manikin also closely simulates the shape of an average person. Four test cases were completed to develop a detailed mapping of the flow conditions around the body. Results are presented for three test cases: baseline velocity and temperature distributions, blockage effect of the unheated manikin, and mixed convection with the heated manikin. An additional test case investigated semi-free convection from the heated manikin in the chamber with low-velocity cooling. Results from the semi-free conduction case are not presented in this article to keep the presentation more focused; however, the reader may refer to Myers (1995) for presentation of results.

EXPERIMENTAL INVESTIGATION

Test Facility

A large environmental chamber designed and fully instrumented for this type of study was used. Test chamber dimensions were 7.3 m × 4.9 m × 2.7 m (24 ft × 16 ft × 9 ft). The test chamber, air handler unit, chiller, air temperature control system, and inlet and return airflow meters used in this study are discussed in detail in Hosni et al. (1994). A high side-wall grille was flush-mounted on the north wall of the chamber and used as the inlet diffuser, as shown in Figure 1a. The grille was placed with its top edge 229 mm (9 in.) below the ceiling and had dimensions of 387 mm × 133 mm (15.25 in. × 5.25 in.) with 19 mm (0.75 in.) spacing and double deflection, fixed airfoil blades set at 90°. Twelve heaters were installed in the chamber floor in three rows and were controlled using a motorized voltage transformer. The four heaters on the row closest to the diffuser and the two side heaters of the middle row were used as a thermal load for testing, as shown in Figure 1b. Thirty-nine thermistors located on the chamber walls, floor, ceiling, and heaters' surfaces, as well as in the inlet and return ducts, were used to measure chamber temperatures.

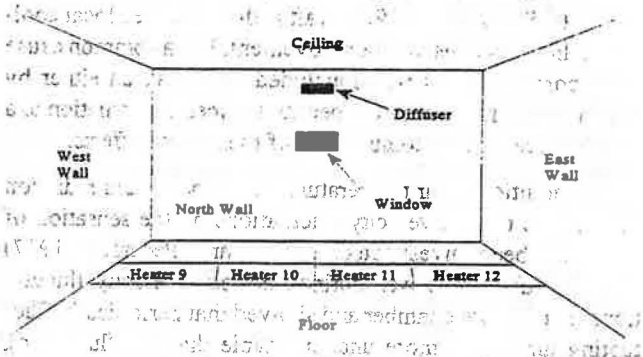

Figure 1a High side-wall grille location in chamber.

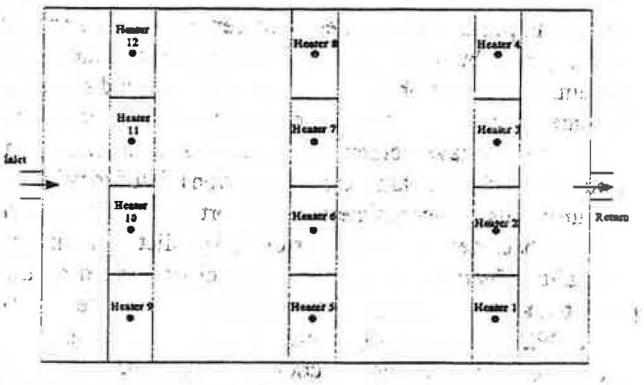

Figure 1b Floor heater layout.

The chamber data acquisition and control system controlled the inlet air temperature and recorded chamber conditions, such as chamber surface and air temperatures, floor heater input power, airflow rates, relative humidity, and mean air velocities from an omnidirectional velocity probe. A probe positioning system, a probe tripod, and thermal anemometry equipment were used to measure velocity and temperature distributions in the chamber, as described in Myers (1995).

Measurement Procedure and Equipment

Prior to each test, the chamber conditions were allowed to reach steady-state conditions and were then recorded. The

steady-state conditions were monitored with the 39 thermistor temperature sensors, the inlet and return airflow meters, and the relative humidity sensor. Previous work by Hawkins et al. (1995) in the chamber was used as a guide for selecting airflow rate and heat load conditions to provide proper velocity and temperature profiles near the manikin location.

A nude thermal manikin was used to simulate the heat load and airflow blockage of a human body in the test chamber and was located standing 4.9 m (16 ft) from the diffuser on the chamber centerline. The thermal manikin was constructed from a light plastic foam casing on top of a metal skeleton. It is a full-size male manikin with 18 electrically separate sections. The nude manikin was heated to standard set temperatures comparable to the surface temperature distribution of each section of the human body. Temperature and power data were recorded from each body segment when the heated thermal manikin was used. Additional information about the thermal manikin and its control system is presented in McCullough and Hong (1994) and McCullough et al. (1994). For this study, the effects of clothing were eliminated by using a nude thermal manikin.

Air velocity and temperature data were collected using two types of sensors in this study. Omnidirectional velocity probes and a thermistor temperature sensor were used to measure mean velocity and temperature in the chamber, respectively. The first low-velocity omnidirectional probe was rated and calibrated for velocity measurements from zero m/s to 1.0 m/s (196 fpm) and was used to measure mean air velocities below 1.00 m/s (196 fpm). The second probe was capable of velocity measurements up to 2.0 m/s (394 fpm) and was used for velocities over 1.00 m/s. The omnidirectional probes have spherical hot-film sensors that are 4.6 mm (0.18 in.) in diameter and are best suited for low-velocity measurements in flow fields where the flow direction is unknown or is difficult to evaluate. The use of any directional type probe such as a three-dimensional probe is not practical since air speed is small and the airflow direction is unclear and unstable. A detailed description of the probes and the calibration procedures are presented in Myers (1995).

A thermal anemometry system with a high-frequency single-sensor hot film probe was also used to measure and record high-frequency variances in air velocity. This system, with its temperature module and a high-frequency thermocouple probe, allowed temperature measurements for temperature compensation of the hot film velocity probe data. The hot-wire probe required a separate computer along with an anemometer and a digitizer, as discussed in Hawkins et al. (1995). The mean velocity data from the thermal anemometry system are not presented in this paper since some velocities were expected to be below the manufacturer-recommended minimum velocity of 0.15 m/s, and the airflow directions were not adequately known for valid measurements. However, the results were compared with the omnidirectional results as a secondary check where mean velocities were greater than 0.15 m/s.

Two types of air velocity and temperature distributions were assembled for this study: (1) chamber profiles and (2) manikin profiles. Measurement procedures for each profile type are briefly described below.

Chamber Profiles. The air velocity and temperature profiles within the chamber, away from the manikin, were assembled from a series of vertically aligned measurement locations using an automated probe-positioning system. The omnidirectional probe, the single-wire hot-film velocity probe, the thermistor and thermocouple probes were all mounted within a close proximity of each other on a probe holder arm of the probe-traversing system. The remote control system allowed for the positioning of the probes at predetermined locations along a vertical axis from floor to ceiling. At each measurement point, the measurement and control program kept the probes in a stationary position for 24 seconds to allow the probes to reach a stable condition prior to initiating the velocity and temperature data collection. Then, 100 readings were taken at 1.25 Hz; however, only 70 readings were used to determine a local mean velocity and temperature. The initial 30 readings were discarded; thus, the integration time for each data point was 56 seconds. ASHRAE recommends a three-minute integration time for this type of sensor. However, the three-minute integration time was too time-consuming due to the large number of measurement locations for each test case. Thus, a study was performed to lower the integration time. The 56-second integration time was found to be acceptable for measurements presented herein. However, when possible, higher integration time is recommended. The mean velocity and temperature data were written to a data file prior to moving the probes to the next measurement position. This procedure was repeated for each complete profile taken from the floor to the ceiling along the chamber centerline and to the left and right of the centerline. Several partial profiles from the manikin head or shoulders to the ceiling were also collected using the same procedure.

Manikin Profiles. The air velocity and temperature measurements close to the manikin skin surface were collected using a probe tripod with the 1.0 m/s (196 fpm) omnidirectional velocity probe and a thermistor probe. A three-axis video camera tripod was modified by the addition of a telescoping probe-holding arm to provide great flexibility and ease of adjustment in locating the velocity probes. Measurement locations for the probe tripod were near the complex surface of the thermal manikin body and, therefore, were aligned by hand and verified by the researcher. Measurements were made using the probe tripod with the same sample rate and period, but waiting times of at least 120 seconds were used to allow the airflow pattern to stabilize. The velocity and temperature data close to the manikin skin surface at various body parts were assembled in tables and circle plots as presented herein.

RESULTS

Results for three test cases are presented in this section. The chamber conditions and the temperature and velocity distributions were measured for each case. The first case includes the baseline velocity and temperature distributions within the chamber without the manikin present. For the second case, the blockage effect of the unheated manikin was investigated in the chamber. The final case examined the mixed convection of the heated manikin in the chamber and the interaction between the thermal plume from the manikin and the room air motion.

Baseline Velocity and Temperature Distributions

In this initial test case, the chamber conditions and the velocity and temperature profiles were measured without the thermal manikin present to obtain a baseline data set for comparison to data with the manikin present. Emphasis was placed on collecting the velocity and temperature profiles in the proximity of the manikin location. Test conditions included inlet and return airflow rates and temperatures, floor heater power and distribution, and chamber surface temperatures. The chamber steady-state temperatures are presented in Figure 2 and listed in Table 1.

The airflow in the chamber was visualized qualitatively by repeatedly injecting smoke into the inlet air duct using a remote control smoke generator. The drop and spread of the cool air jet were observed using smoke flow visualization techniques to verify qualitatively that proper air distribution was present. Two views of the observed airflow patterns are presented in Figure 3. The cool air jet remained continuous from the diffuser to the return and stayed mostly along the centerline. Most of the lateral jet spread was observed to be within a width of 2.4 m (8 ft), leaving a margin of 1.2 m (4 ft) on either side of the chamber. While some of the air mixed thoroughly, most of the smoke was carried out of the room by the return. The upper side of the cool air jet attached to the ceiling at about 0.5 m (20 in.) from the diffuser located in the north wall and separated from the ceiling just behind the middle row of floor heaters. The lower boundary of the cool air jet entrained air from the front of the room through the bottom of the jet, and the jet fell to the floor 4.15 m (13.6 ft) from the

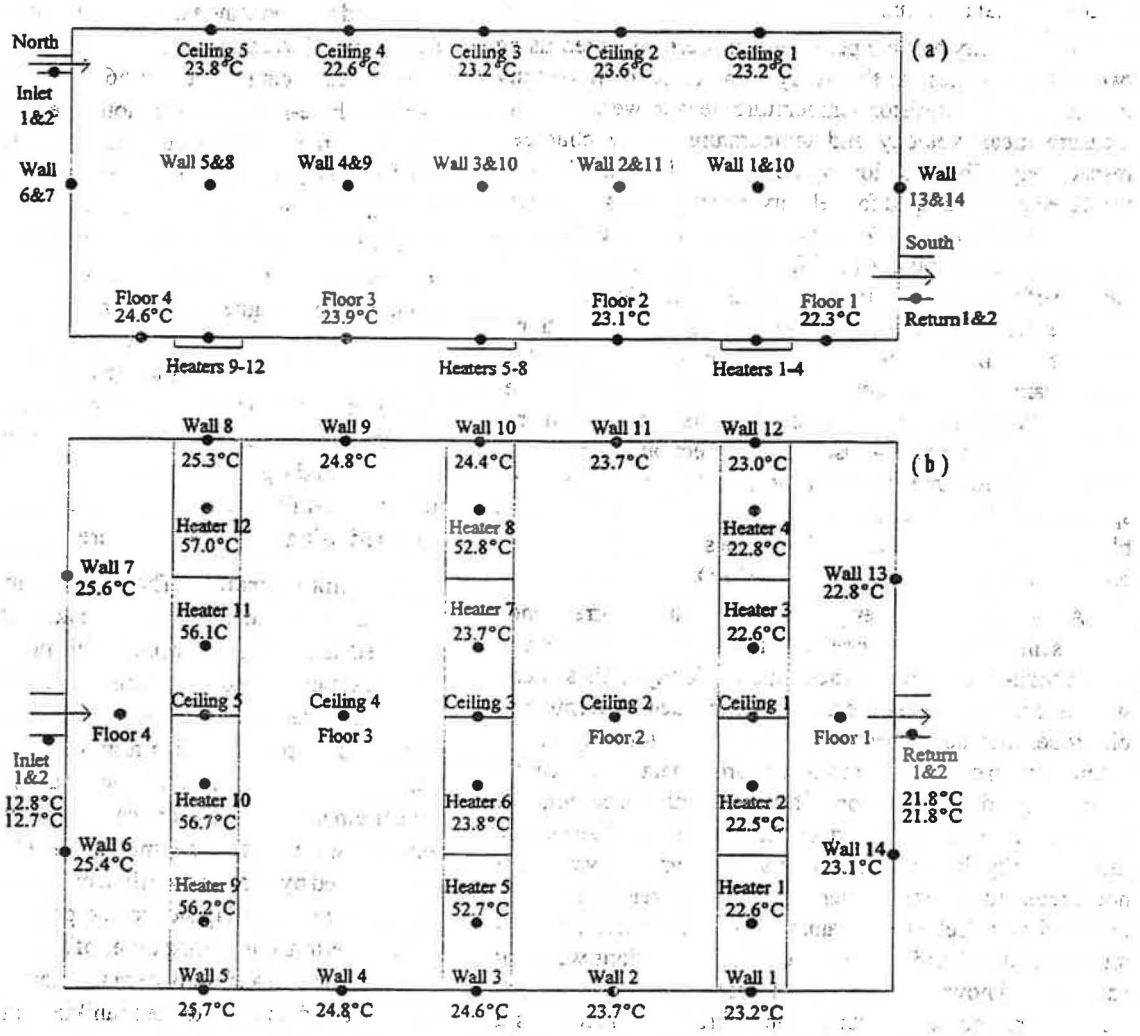

Figure 2 Steady-state chamber temperatures and corresponding thermistor locations without the thermal manikin: (a) front view, (b) top view.

TABLE 1
Steady-State Temperatures for the Three Test Cases

Thermistor Location	Case #1 Temp.°C	Case #1 Temp.°F	Case #2 Temp.°C	Case #2 Temp.°F	Case #3 Temp.°C	Case #3 Temp.°F
Inlet-1	12.8	55.0	12.5	54.5	12.2	54.0
Inlet 2	12.7	54.8	12.4	54.3	12.1	53.8
Return 1	21.8	71.3	21.5	70.7	22.8	73.0
Return 2	21.8	71.3	21.5	70.8	22.7	72.9
Floor 1	22.3	72.2	22.1	71.8	23.6	74.6
Floor 2	23.1	73.5	22.1	71.7	24.3	75.7
Floor 3	23.9	75.0	23.7	74.7	25.1	77.1
Floor 4	24.6	76.3	24.4	75.9	25.8	78.5
Heater 1	22.6	72.6	22.4	72.4	23.9	75.0
Heater 2	22.6	72.6	22.4	72.3	24.0	75.2
Heater 3	22.6	72.7	22.5	72.5	23.9	75.1
Heater 4	22.8	73.0	22.6	72.6	23.9	75.0
Heater 5	52.7	126.9	53.1	127.5	55.0	131.0
Heater 6	23.8	74.9	23.5	74.2	24.9	76.8
Heater 7	23.7	74.7	23.6	74.4	24.8	76.7
Heater 8	52.8	127.1	52.9	127.2	54.1	129.4
Heater 9	56.2	133.2	56.6	134.0	58.0	136.4
Heater 10	56.7	134.1	57.0	134.5	58.0	136.3
Heater 11	56.1	132.9	56.0	12.5	55.8	132.4
Heater 12	57.0	134.6	57.2	134.9	58.0	136.5
Ceiling 1	23.2	73.8	23.1	73.6	24.8	76.7
Ceiling 2	23.6	74.4	23.0	73.5	24.7	76.4
Ceiling 3	23.2	73.8	23.3	73.9	24.7	76.4
Ceiling 4	22.6	72.7	22.7	72.8	23.9	75.1
Ceiling 5	23.8	74.8	23.9	75.0	25.1	77.2
Wall 1	23.3	73.9	22.9	73.2	24.5	76.1
Wall 2	23.7	74.6	23.4	74.1	25.0	76.9
Wall 3	24.6	76.3	24.4	75.8	25.9	78.7
Wall 4	24.8	76.7	24.6	76.3	26.0	78.8
Wall 5	25.7	78.3	25.5	77.9	26.9	80.4
Wall 6	25.4	77.7	25.3	77.5	26.7	80.1
Wall 7	25.6	78.1	25.5	77.8	26.9	80.4
Wall 8	25.4	77.6	25.3	77.6	26.6	79.9
Wall 9	24.8	76.6	24.6	76.3	26.1	78.9
Wall 10	24.4	75.9	24.2	75.6	25.7	78.3
Wall 11	23.7	74.6	23.5	74.2	25.0	77.0
Wall 12	23.0	73.3	22.6	72.7	24.3	75.7
Wall 13	22.9	73.1	22.7	72.9	24.3	75.7
Wall 14	23.1	73.5	22.8	73.1	24.4	75.9
Airflow Rate	137 (L/s)	290 (cfm)	137 (L/s)	290 (cfm)	137 (L/s)	290 (cfm)
Heater Power	1600 (W)	5460 (Btu/h)	1600 (W)	5460 (Btu/h)	1600 (W)	5460 (Btu/h)

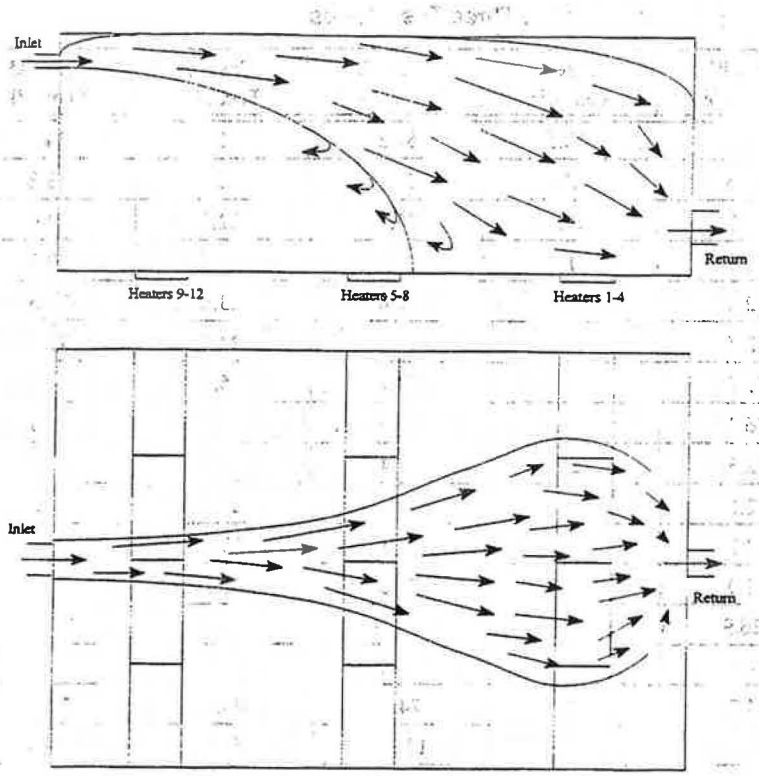

Figure 3 Smoke flow visualization results within the chamber without the manikin.

diffuser at 0.15 m (6 in.) behind the second row of floor heaters.

The velocity profiles were normalized by the maximum velocity, 0.86 m/s (170 fpm), observed at an axial location of 4000 mm (157 in.) from the diffuser at a vertical location of 2100 mm (83 in.) from the floor on the chamber centerline. Since each normalized velocity is based on a local mean velocity from the omnidirectional velocity probe, no specific direction or angular inclination for the velocities should be inferred from the velocity profiles. The flow visualization observations are the best indication of the direction of room airflow.

The normalized temperature, T_{norm}, was calculated from the local mean temperature, T, the inlet temperature, T_{inlet}, the return temperature, T_{return}, and an expansion factor, C. The expansion factor, C, was a constant multiplier (2.5), which was used to widen the range of normalized temperatures for ease in comparing and contrasting profiles. The normalized temperature was defined as the ratio of the difference between the local mean temperature and the inlet temperature to the difference between the return and inlet temperatures. The inlet and return temperatures were 12.8°C (55.0°F) and 21.8°C (71.3°F), respectively. Normalized temperatures vary from 0.0 to 1.0, where values less than 0.5 indicate cooler temperatures, and values greater than 0.5 indicate warmer temperatures.

The normalized velocity and temperature profiles along the chamber centerline are presented in Figures 4a and 5a. The x-axis in the figures shows the distance away from the diffuser along the chamber centerline. The y-axis represents the height from floor to the ceiling. Solid vertical reference lines are placed between each profile, and dotted vertical reference lines represent a value of 0.5. Horizontal dotted reference lines indicate the height of the manikin head, shoulder, hip, and knee. Although the manikin was not used in this case, the lines are provided as a basis for comparison in the occupied zone of the chamber.

Both the velocities and temperatures show the shape and strength of the air jet from the higher velocities and cooler temperatures expected in the jet. The jet expanded so that the peak velocity was 600 mm (24 in.) from the ceiling at 4000 mm (157 in.) from the diffuser. The peak velocities continued to descend from the ceiling and decreased in magnitude as the jet moved toward the return. The velocities below the manikin head level increased compared to the peak velocities as the jet moved toward the return.

The temperature profiles show behaviors similar to the velocity profiles. From 4600 mm (181 in.) from the diffuser back toward the return, minimum normalized temperatures became closer to 0.5, and the normalized temperatures generally became cooler and more uniform in the occupied zone below manikin head level at 1700 mm (67 in.). These results indicate that the jet was expanding downward and mixing well with the room air from 4600 mm (181 in.) from the diffuser back to the return.

Normalized velocity and temperature profiles in the transverse direction at a location 4900 mm (193 in.) from the diffuser are given in Figures 4b and 5b. Decreased velocities and increased temperatures left and right of the centerline show the effect of the expanded jet region at this distance from the diffuser. Figures 4c and 5c present a similar plot of normalized velocity and temperature profiles 5050 mm (199 in.) from the diffuser. Both velocities and temperatures at this transverse location were similar to those at 4900 mm (193 in.) from the diffuser.

Blockage Effect of the Unheated Manikin

The second test case builds on the first case, investigating the blockage effect of the unheated thermal manikin. Chamber temperature conditions were comparable to those for the first test case without the manikin, as listed in Table 1. Chamber airflow was qualitatively visualized by two methods for this test case. The smoke flow visualization method used in the previous case was repeated, as shown in Figure 6. Visualization was also performed by releasing low-velocity smoke from the smoke generator near the manikin. The low-velocity smoke enhanced the observation of local flow phenomena, as presented in Figure 7.

The elevation view of the chamber airflow pattern shows phenomena similar to the previous case. Cool inlet air attached

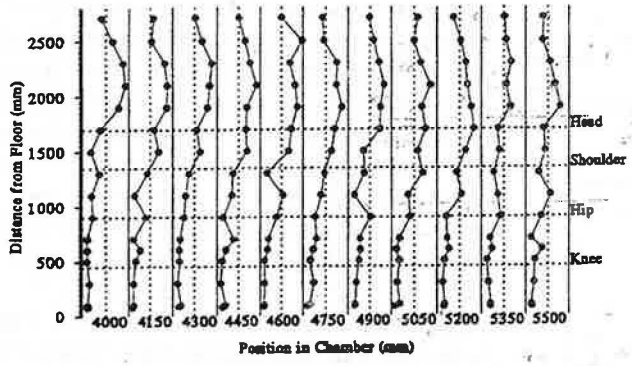

(a) Profiles along the chamber centerline.

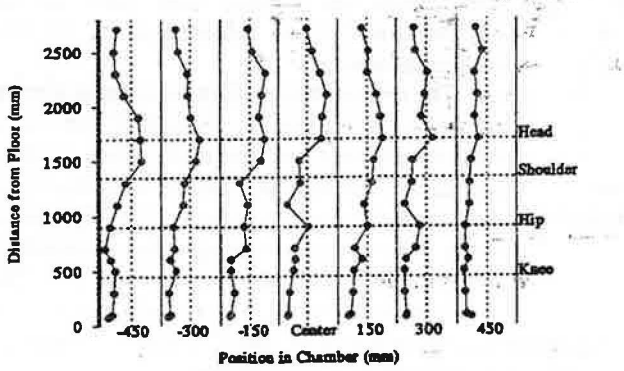

(b) Profiles in the transverse direction at 4900 mm.

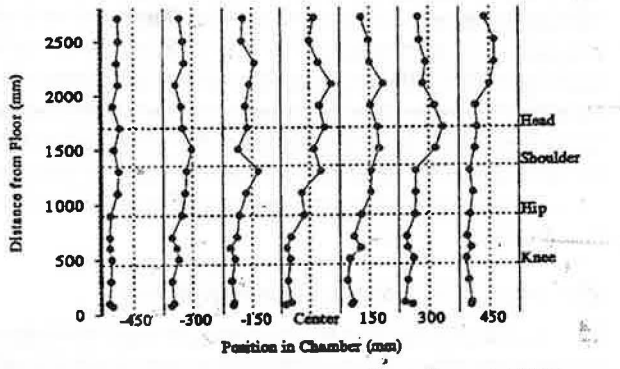

(c) Profiles in the transverse direction at 5050 mm.

Figure 4 *Normalized velocity profiles within the chamber without the manikin.*

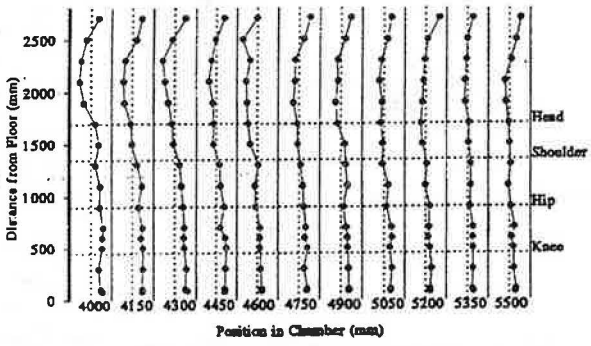

(a) Profiles along the chamber centerline.

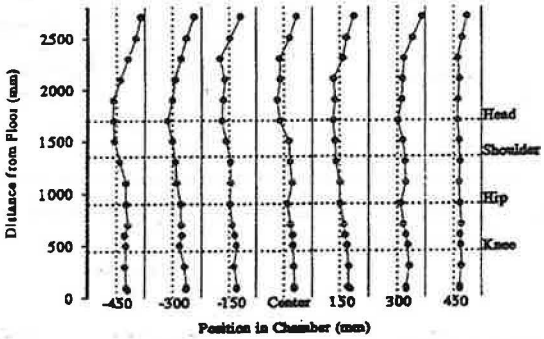

(b) Profiles in the transverse direction at 4900 mm.

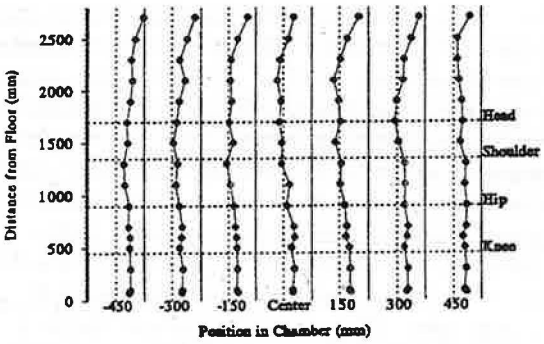

(c) Profiles in the transverse direction at 5050 mm.

Figure 5 *Normalized temperature profiles within the chamber without the manikin.*

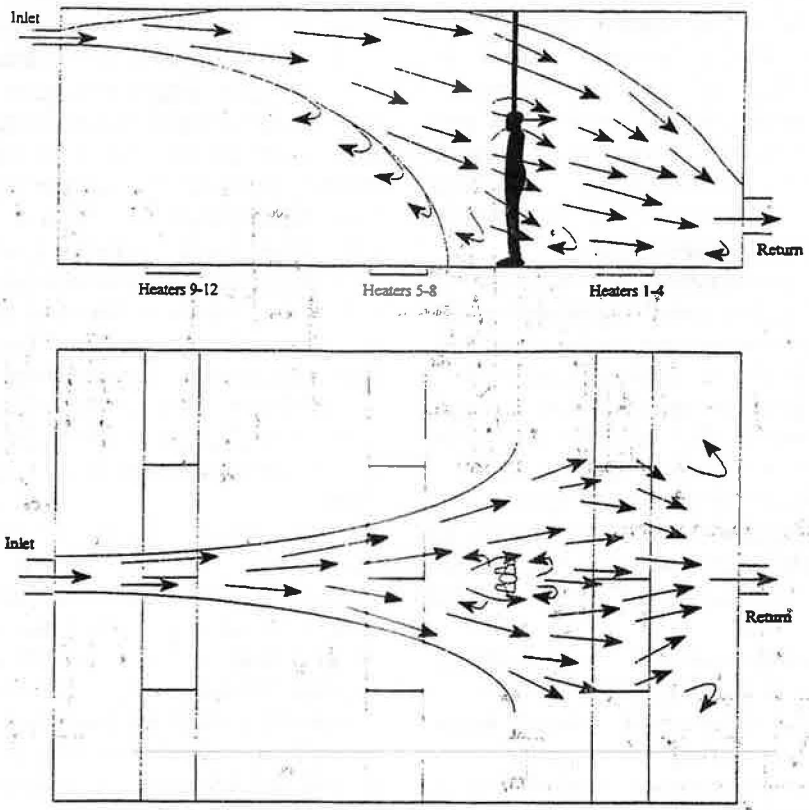

Figure 6 *Smoke flow visualization results for the blockage effect of the unheated manikin.*

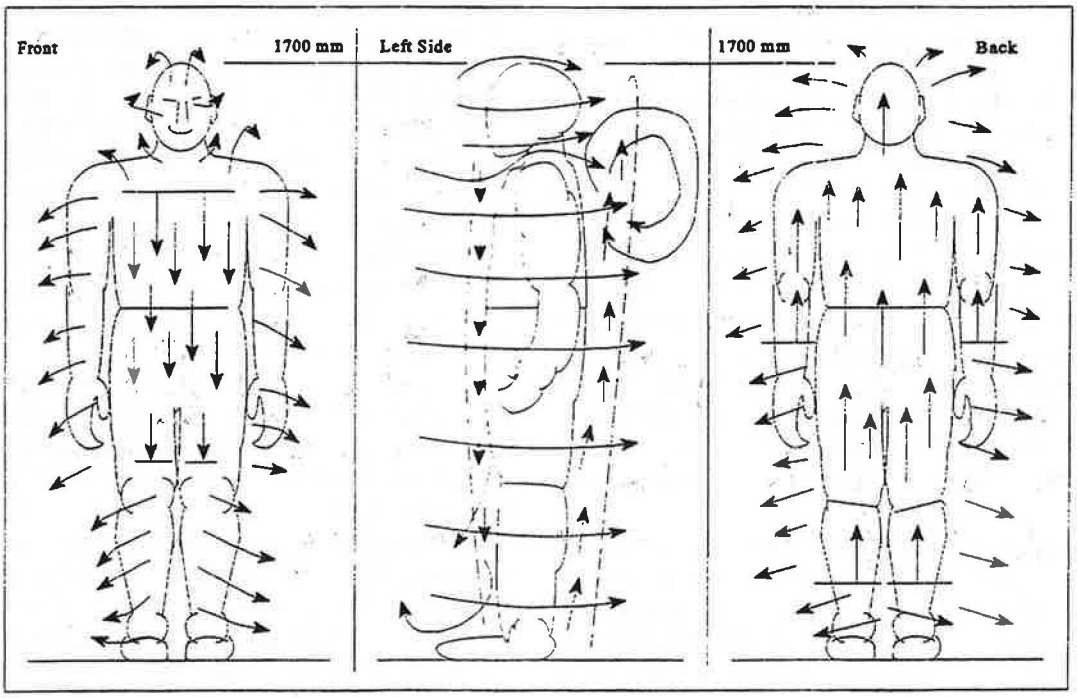

Figure 7 *Local airflow patterns near the thermal manikin for the blockage effect of the unheated manikin.*

to the ceiling, but the jet region descended more directly from the ceiling to the return behind the manikin. The jet region expanded across a wider section of the chamber than in the first test case. Recirculation patterns were observed near the shoulders, neck, and ankles of the thermal manikin. The three views of the unheated thermal manikin in Figure 7 show the observed patterns of airflow near the manikin from flow visualization. A repeatable recirculation region was observed behind the back of the thermal manikin.

Normalized velocity and temperature profiles (Figures 8 and 9) were constructed from local mean velocity and temperature data measured by the omnidirectional velocity and thermistor probes. The presence of the thermal manikin interfered with some measurement locations used in the first test case. Velocity and temperature profiles for 4900 mm (193 in.) from the diffuser were measured at 150 mm (6 in.) left and right of the centerline and at 4970 (196 in.) from the diffuser on the centerline. Measurement locations were moved from behind the manikin at 5050 mm (199 in.) on the centerline to 5080 mm (200 in.) from the diffuser to ensure the safety of the manikin and the sensors.

The velocity profiles were normalized by the maximum velocity for this test case, 0.86 m/s (170 fpm), which was measured at 4000 mm (157 in.) from the diffuser and 2100 mm (83 in.) from the floor on the centerline. The maximum velocity for this case was the same as in the previous case without the thermal manikin. Normalized temperatures, T_{norm}, were calculated in the same manner as in the first test case. The inlet and return temperatures were 12.5°C (54.5°F) and 21.5°C (70.7°F).

Normalized velocity and temperature profiles for the centerline are presented in Figures 8a and 9a. The velocities in front of and above the thermal manikin are similar to those of the previous case. At 5080 mm (200 in.) from the diffuser, velocities were lower than in the previous case from manikin hip level at 900 mm (35 in.) from the floor to head level at 1700 mm (67 in.). These decreased velocities were the direct result of the manikin blockage. Velocities at comparable locations in front of the manikin were measured with the probe tripod.

The normalized temperature profiles at 4000 mm, 4600 mm, 4900 mm, and 5200 mm (157 in., 181 in., 193 in., and 205 in.) from the diffuser were similar to previous results. The temperatures at 4750 mm (187 in.), 150 mm (6 in.) in front of the manikin, were lower than the previous values, while the temperatures at 5080 mm (200 in.) were higher than previous values.

The normalized velocity and temperature profiles left and right of the centerline at 4900 mm (193 in.) from the diffuser are presented in Figures 8b and 9b. Those profiles were very similar to the profiles of the previous case. Normalized velocity and temperature profiles left and right of the centerline at 5080 mm (196 in.) from the diffuser are shown in Figures 8c and 9c. At 5080 mm (199 in.), velocities at 150 mm (6 in.) left and right of the centerline were lower from the manikin hip at 900 mm (35 in.) to the head at 1700 mm (67 in.) than comparable velocities from the previous test case, which again illustrates the blockage of the thermal manikin. Temperature profiles for this location were similar to previous results.

The probe tripod was used to measure the temperature and velocity distributions near the manikin skin surface. The probes were located 10 mm to 50 mm (0.4 in. to 2.0 in.) from the body at 10 mm (0.4 in.) intervals on 90 axes around the body. Measurements were taken at the following body locations: ankles, thighs, hip and lower arm, chest, back, point and top of shoulders, and crown of head. Probe locations for data collected with the probe tripod are identified by the direction and distance from the body part. The directions are front, left, back, right, and top. All of these data were placed in the form of circular plots (Myers 1995); an example of the circular plots is presented in Figure 10. Due to space limitations, these plots are not reproduced here. Instead, the data are presented in Table 2.

Velocity and temperature data for the measurements taken at 100 mm (4 in.) from the floor near the ankles of the unheated manikin show that the velocities on the front and back of the ankles were lower than those on the sides of the ankles. The air velocity increased as it moved around the body segment. Temperature readings were higher on the back and outside of the ankles and lower on the front and inside of the ankles. Lower velocities on the back and outside of the ankles allowed higher temperatures in the calmer air due to the manikin blockage.

The velocity and temperature data for the thighs (600 mm, 24 in. above the floor) of the manikin showed noticeably higher velocities at this height than at the ankles, while temperatures decreased. The velocity readings for the lower arms of the thermal manikin at 900 mm (35 in.) from the floor were higher around the lower arms than the thighs. Lower temperature readings accompanied the higher velocities on the inside of the lower arms between the arms and the hips.

Velocity and temperature results for the hips at 900 mm (35 in.) from the floor show 15 measurement locations around the front, side, and back of each hip. These measurements and the data along the chamber centerline near the abdomen and back of the thermal manikin show lower velocities along the back due to blockage effects.

The data for the shoulders, chest, and back of the thermal manikin at 1300 mm and 1400 mm (51 in. and 55 in.) above the floor in Table 2 show that the velocities were highest above and to the sides of the body and lowest at the back. Temperatures were cooler in front of the chest and increased around the body to the back. Velocities increased from the torso to the shoulders, while temperatures decreased as the cool, fast chamber airflow deflected around the manikin.

In summary, the blockage of the unheated manikin was observed through consistently lower velocity readings behind every body part. Mean temperatures were higher behind the manikin because less mixing occurred there. The front and sides of the manikin were cooled more than the back by the chamber airflow, as evidenced by higher velocities and lower

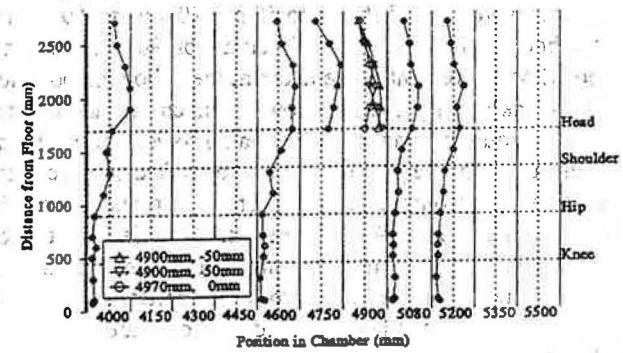

(a) Profiles along the chamber centerline.

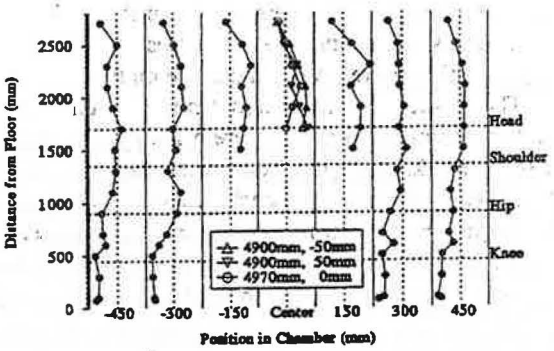

(b) Profiles in the transverse direction at 4900 mm.

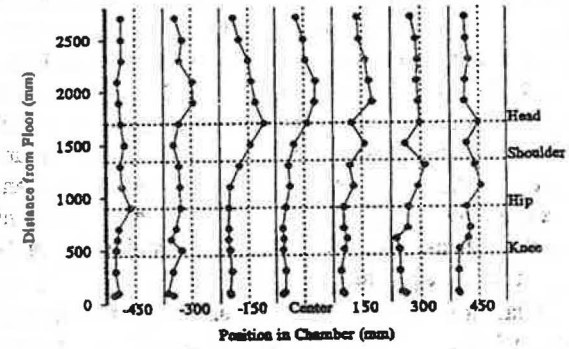

(c) Profiles in the transverse direction at 5050 mm.

Figure 8 *Normalized velocity profiles within the chamber with the unheated manikin.*

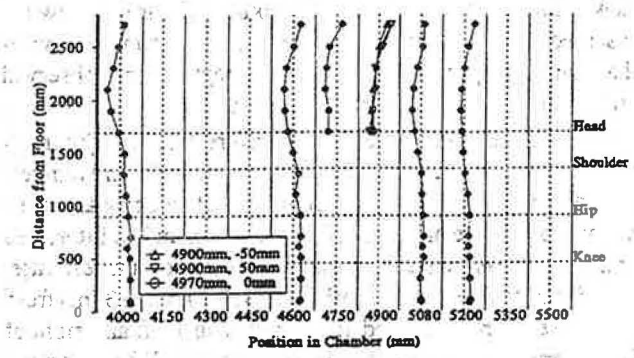

(a) Profiles along the chamber centerline.

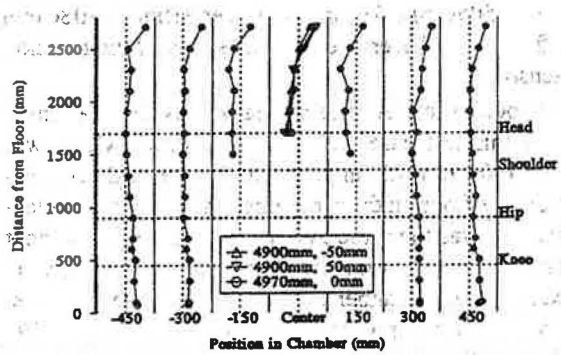

(b) Profiles in the transverse direction at 4900 mm.

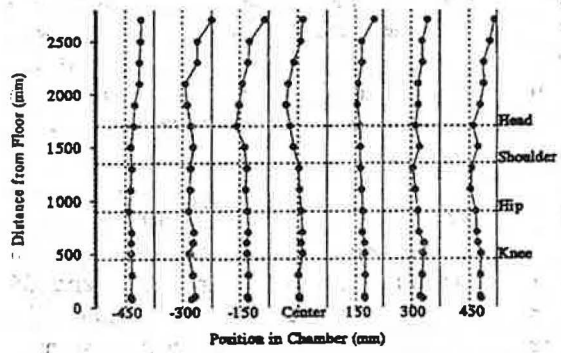

(c) Profiles in the transverse direction at 5080 mm.

Figure 9 *Normalized temperature profiles within the chamber with the unheated manikin.*

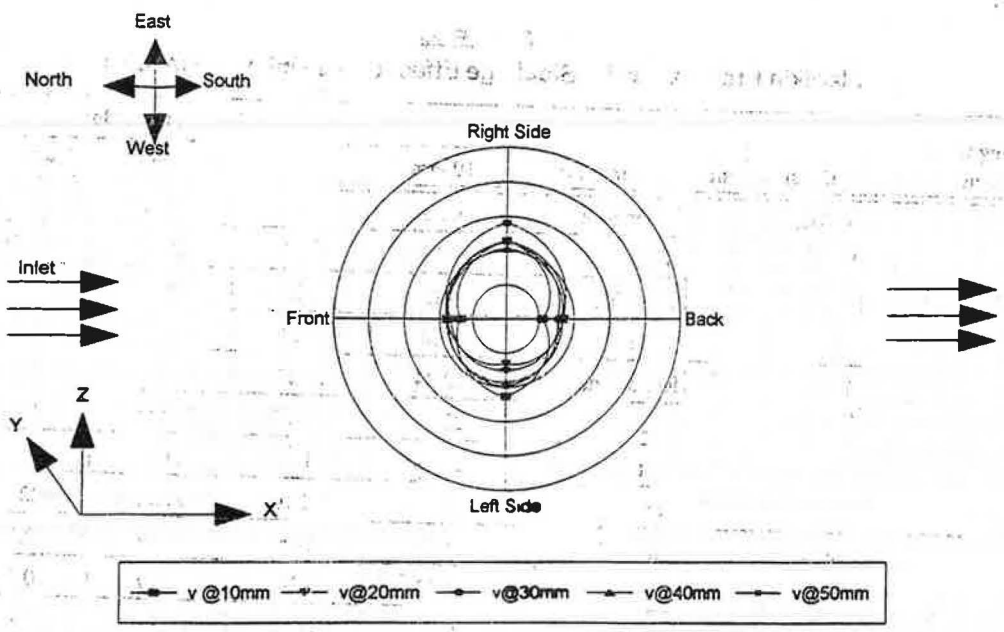

***Figure 10** An example of velocity circle plot from the right ankle for the blockage effect of the unheated manikin.*

temperatures. In many areas on the front of the manikin, lower velocity stagnation zones were observed because the velocities on these regions were lower than velocities for the sides of the same body parts.

Mixed Convection with the Heated Manikin

For the final test case, the interaction of the chamber air motion with the thermal plume from the heated manikin was investigated. The position of the manikin was kept the same as in the previous case with similar chamber thermal and ventilation conditions. The combination of free convection from the heated thermal manikin and forced convection due to the chamber air motion created mixed convection conditions. Chamber temperature conditions were established such that they were similar to previous cases presented in Table 1. The total power to the heated thermal manikin was set at 164 W (561 Btu/h) to represent a person with a modest activity level (1.5 met). The distribution of the heat loss over the manikin surface was determined by the manikin's heaters and, to a reasonable approximation, represents the heat distribution of a person. Temperatures and power levels for each manikin segment for this test case are presented in Table 3.

The two qualitative smoke flow visualization methods used in the previous unheated manikin case were used to observe the airflow patterns within the chamber and close to the manikin, as presented in Figures 11 and 12. The spread and drop of the cool air jet were between the extremes of the two previous cases. Differences between jet behavior for this case and previous cases were caused by the thermal plume from the heated manikin. This phenomenon would cause the cool air jet to detach from the ceiling closer to the diffuser, drop to the floor farther from the diffuser, and expand to a lesser width across the chamber than in the manikin blockage case No. 2. While most of the chamber air was deflected around the thermal manikin, a boundary layer formed around the thermal manikin. The flow direction of the boundary layer appeared to be up the back of the body and down the front. Recirculation patterns similar to those previously identified were observed.

Velocity and temperature profiles within the chamber were collected at the same measurement locations as the manikin blockage case No. 2. Velocity profiles were normalized by the maximum velocity found near the thermal manikin for this case, 0.93 m/s (183 fpm), which was found at 4000 mm (157 in.) from the diffuser at 2100 mm (83 in.) above the floor on the centerline. Mean velocities for this case, as presented in normalized profiles, were 8% greater than velocities from the unheated manikin blockage case. Normalized temperatures were determined using the same calculation procedure as in earlier test cases. For this test case, inlet and return temperatures were 12.2°C (54.0°F) and 22.7°C (72.9°F), respectively.

Normalized velocity and temperature profiles for the centerline are presented in Figures 13a and 14a. Velocity profiles at 4000 mm, 4600 mm, 4750 mm, and 4900 mm (157 in., 181 in., 187 in., and 193 in.) from the diffuser were very similar to those of the second test case at the same locations. Velocity profiles at 5080 mm and 5200 mm (200 in. and 205 in.) from the diffuser showed peak velocities at locations closer to the head of the manikin (1700 mm, 67 in. above the floor), rather than at 2100 mm (83 in.) from the floor, as in the manikin blockage case. In this case, buoyant forces pulled the cool air jet down from the ceiling toward the south wall to a greater degree as the jet encountered the warm region in the thermal plume above the thermal manikin, while the unheated manikin of case No. 2 deflected airflow over the head of the manikin and kept peak velocities in each profile farther from the floor. Temperature profiles on the centerline were gener-

TABLE 2a
Manikin Profiles for the Blockage Effect of the Unheated Manikin

Body Segment and Elevation	Measurement	Direction	Distance from Body				
			10 mm	20 mm	30 mm	40 mm	50 mm
Right Ankle 100 mm	Velocity (m/s)	Right Side	0.23	0.23	0.28	0.21	0.23
		Back	0.11	0.17	0.16	0.16	0.15
		Left Side	0.23	0.13	0.15	0.19	0.20
		Front	0.14	0.18	0.17	0.18	0.17
	Temperature (°C)	Right Side	22.24	22.31	22.29	22.28	22.33
		Back	22.21	22.17	22.16	22.22	22.21
		Left Side	21.69	21.80	21.85	21.78	21.77
		Front	22.13	22.10	22.15	22.11	22.18
Right Thigh 600 mm	Velocity (m/s)	Right Side	0.16	0.16	0.19	0.13	0.14
		Back	0.09	0.10	0.10	0.15	0.13
		Left Side	0.37	0.38	–	–	–
		Front	0.31	0.43	0.38	0.37	0.27
	Temperature (°C)	Right Side	21.32	21.36	21.43	21.65	21.60
		Back	21.69	21.60	21.54	21.51	21.54
		Left Side	21.57	21.49	–	–	–
		Front	21.54	21.38	21.37	21.25	21.42
Right Lower Arm 900 mm	Velocity (m/s)	Right Side	0.20	0.55	0.50	0.44	0.53
		Back	0.17	0.20	0.25	0.22	0.13
		Left Side	0.67	–	–	–	–
		Front	0.46	0.52	0.40	0.53	0.44
	Temperature (°C)	Right Side	21.84	21.86	21.85	21.84	21.87
		Back	21.88	21.91	21.90	21.86	21.90
		Left Side	21.76	–	–	–	–
		Front	21.90	21.83	21.92	21.88	21.88
Hip 900 mm	Velocity (m/s)	Front	0.44	0.47	0.46	0.40	0.38
		Right Hip Front	0.44	0.47	0.55	0.50	0.23
		Right Hip Right	0.67	–	–	–	–
		Right Hip Back	0.14	0.21	0.19	0.22	0.22
		Back	0.13	0.17	0.25	0.19	0.22
	Temperature (°C)	Front	21.39	21.36	21.45	21.57	21.66
		Right Hip Front	21.94	21.79	21.73	21.79	22.04
		Right Hip Right	21.76	–	–	–	–
		Right Hip Back	21.87	21.84	21.79	21.83	21.83
		Back	21.72	21.79	21.67	21.82	21.83

TABLE 2a (Continued)
Manikin Profiles for the Blockage Effect of the Unheated Manikin

Body Segment and Elevation	Measurement	Direction	Distance from Body				
			10 mm	20 mm	30 mm	40 mm	50 mm
Shoulder 1300 mm	Velocity (m/s)	Chest	0.36	0.37	0.34	0.36	0.29
		Right Shoulder	0.35	0.53	0.59	0.63	0.46
		Back	0.19	0.26	0.28	0.24	0.25
	Temperature (°C)	Chest	21.38	21.34	21.38	21.28	21.48
		Right Shoulder	21.57	21.65	21.58	21.49	21.64
		Back	21.81	21.77	21.77	21.75	21.75
Top of Shoulder 1400 mm	Velocity (m/s)	Front Top	0.54	0.44	0.51	0.52	0.41
		Right Top	0.76	0.67	0.72	0.78	0.76
		Back Top	0.34	0.35	0.33	0.38	0.38
	Temperature (°C)	Front Top	21.51	21.52	21.43	21.52	21.51
		Right Top	21.30	21.35	21.32	21.24	21.29
		Back Top	21.19	21.29	21.25	21.30	21.51
Crown of Head 1700 mm	Velocity (m/s)	Front	0.74	0.64	0.68	0.54	0.58
		Right Side	0.91	0.67	0.79	0.66	0.94
		Back	0.27	0.31	0.40	0.43	0.47
	Temperature (°C)	Front	21.39	21.35	21.39	21.52	21.46
		Right Side	20.35	20.47	20.41	20.51	20.32
		Back	21.39	21.51	21.40	21.54	21.46

TABLE 2b
Manikin Profiles for the Mixed Convection with the Heated Manikin

Body Segment and Elevation	Measurement	Direction	Distance from Body				
			10 mm	20 mm	30 mm	40 mm	50 mm
Right Ankle 100 mm	Velocity (m/s)	Right Side	0.14	0.20	0.15	0.24	0.27
		Back	0.17	0.17	0.21	0.24	0.27
		Left Side	0.27	0.30	0.32	0.30	0.24
		Front	0.22	0.23	0.22	0.15	0.20
	Temperature (°C)	Right Side	23.84	23.83	23.85	23.76	23.69
		Back	23.94	24.07	24.08	24.04	24.07
		Left Side	23.98	24.32	24.28	24.13	24.22
		Front	23.56	23.80	23.78	23.72	23.81
Right Thigh 600 mm	Velocity (m/s)	Right Side	0.18	0.14	0.34	0.14	0.24
		Back	0.14	0.19	0.16	0.15	0.20
		Left Side	0.57	0.53			
		Front	0.56	0.53	0.27	0.51	0.46
	Temperature (°C)	Right Side	24.67	24.88	24.84	24.67	24.73
		Back	24.19	24.48	24.58	24.59	24.60
		Left Side	25.13	25.08			
		Front	23.86	23.68	23.66	23.64	23.74

TABLE 2b (Continued)
Manikin Profiles for the Mixed Convection with the Heated Manikin

Body Segment and Elevation	Measurement	Direction	Distance from Body				
			10 mm	20 mm	30 mm	40 mm	50 mm
Right Lower Arm 900 mm	Velocity (m/s)	Right Side	0.22	0.37	0.60	0.65	0.62
		Back	0.20	0.29	0.23	0.24	0.22
		Left Side	0.80				
		Front	0.72	0.58	0.62	0.43	0.49
	Temperature (°C)	Right Side	23.83	23.73	23.51	23.51	23.64
		Back	24.11	24.11	24.14	24.24	24.28
		Left Side	24.92				
		Front	23.74	23.71	23.62	23.66	23.67
Hip 900 mm	Velocity (m/s)	Front	0.52	0.59	0.68	0.54	0.57
		Right Hip Front	0.60	0.60	0.49	0.57	0.62
		Right Hip Right	0.80				
		Right Hip Back	0.27	0.27	0.25	0.29	0.24
		Back	0.20	0.35	0.26	0.32	0.29
	Temperature (°C)	Front	23.61	23.44	23.29	23.43	23.40
		Right Hip Front	23.62	23.57	23.61	23.62	23.62
		Right Hip Right	24.92				
		Right Hip Back	24.72	24.68	24.68	24.53	24.45
		Back	24.82	24.96	24.88	24.84	24.97
Shoulder 1300 mm	Velocity (m/s)	Chest	0.45	0.39	0.37	0.35	0.37
		Right Shoulder	0.44	0.71	0.51	0.77	0.60
		Back	0.28	0.35	0.33	0.29	0.28
	Temperature (°C)	Chest	23.83	23.31	23.17	23.22	23.12
		Right Shoulder	23.24	23.38	23.50	23.52	23.51
		Back	24.72	24.71	24.67	24.52	24.49
Top of Shoulder 1400 mm	Velocity (m/s)	Front Top	0.60	0.40	0.52	0.52	0.47
		Right Top	0.52	0.79	0.59	0.50	0.73
		Back Top	0.26	0.26	0.29	0.33	0.40
	Temperature (°C)	Front Top	23.46	23.49	23.37	23.40	23.35
		Right Top	23.29	23.22	23.29	23.39	23.08
		Back Top	23.59	23.64	23.79	23.69	23.64
Crown of Head 1700 mm	Velocity (m/s)	Front	0.74	0.62	0.61	0.64	0.72
		Right Side	0.96	0.85	0.84	0.70	0.80
		Back	0.30	0.30	0.28	0.36	0.36
	Temperature (°C)	Front	22.73	22.76	22.85	22.79	22.64
		Right Side	23.03	23.16	23.23	23.39	23.16
		Back	22.86	22.89	22.91	22.94	22.91

TABLE 3
Temperatures and Power Input to Heated Thermal Manikin Segments for the Mixed Convection Test Case

Manikin Segment	#	Area		Temperature		Power	
		cm^2	$in.^2$	°C (± 0.1)	°F (± 0.18)	W	Btu/h
Head	1	1329	523	28.3	82.9	11.28	38.50
Chest	2	1888	743	30.6	87.1	19.17	65.43
Back	3	1929	759	32.4	90.3	19.02	64.92
Left Upper Arm	4	1066	420	30.9	87.6	10.17	34.71
Right Upper Arm	5	1051	414	30.1	86.2	10.57	36.08
Left Lower Arm	6	556	219	30.8	87.4	5.51	18.81
Right Lower Arm	7	547	215	30.7	87.3	5.54	18.91
Left Hand	8	441	174	29.5	85.1	2.83	9.66
Right Hand	9	419	165	29.5	85.1	2.37	8.09
Left Thigh	10	1634	643	31.4	88.5	13.82	47.17
Right Thigh	11	1652	650	31.6	88.9	14.42	49.22
Left Calf	12	1056	416	31.5	88.7	10.03	34.23
Right Calf	13	1036	408	31.6	88.9	9.91	33.82
Left Foot	14	653	257	29.6	85.3	2.54	8.67
Right Foot	15	643	253	29.5	85.1	2.32	7.92
Stomach	16	1095	431	31.7	89.1	11.28	38.50
Lap	17	366	144	32.9	91.2	4.80	16.38
Buttocks	18	844	332	32.3	90.1	8.83	30.14
Total		18205	7167	30.8	87.4	164.41	561.13

ally similar to those from the manikin blockage case. Higher normalized temperatures in front of the manikin were the result of the peak velocity flow of the cool air jet descending more precipitously toward the floor in front of the manikin.

Normalized velocity and temperature profiles at 4900 mm (193 in.) from the diffuser, in the transverse direction, are shown in Figures 13b and 14b. At 150 mm (6 in.) left and right of the centerline, velocity and temperature readings were greater above the manikin than in case No. 2. Velocity and temperature profiles at 300 mm and 450 mm (12 in. and 18 in.) left and right of the centerline were similar to those compiled for the manikin blockage case. Figures 13c and 14c present normalized velocity and temperature profiles for 5080 mm (200 in.) from the diffuser. The velocity and temperature profiles at this location again illustrate the airflow blockage due to the manikin at the centerline and at 150 mm (6 in.) left and right of the centerline.

Examination of the mixed convection from the heated thermal manikin concluded with the observation of the flow conditions near the skin surface of the thermal manikin. The velocity and temperature data are presented in Table 2b. For the data taken at 100 mm (4 in.) from the floor near the ankles, velocities followed the trend from the manikin blockage case No. 2. Temperature readings were greater for this case than for the blockage case. The velocity and temperature data for the thighs (600 mm, 24 in. above the floor) of the thermal manikin exhibited patterns similar to the velocity trends around the thighs for case No. 2. For the lower arms of the thermal manikin at 900 mm (35 in.) from the floor, velocities were also similar to the previous test case. Temperatures were lower than for the thighs but similar for the lower arms as compared to case No. 2. Velocity and temperature distributions around the hips and body at 900 mm (35 in.) from the floor in Table 2b show comparable velocities to those found around the hips and body in case No. 2. The velocity and temperature magnitudes around the hips and body were comparable to readings around the thighs for this case. The velocity and temperature data around the shoulders, chest, and back of the thermal manikin at 1300 mm and 1400 mm (51 in. and 55 in.) above the floor show stagnation in front of the chest, which caused velocities in front of the body to be similar to those behind the body, while chamber air was deflected around the points of the shoulders with higher velocities. Temperatures in front of the manikin and at the points of the shoulders were lower than behind the manikin. The velocities in front of the chest were lower than those in front of the manikin at the hips (900 mm, 35 in. from the floor), while readings at the back were similar to those at the back near the hips. Velocities over the top of the

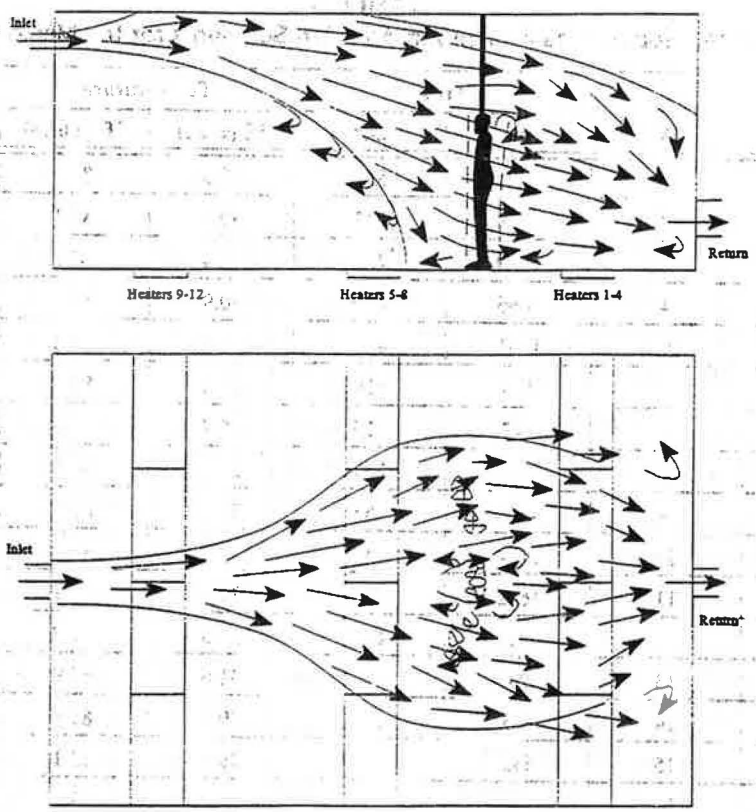

Figure 11 *Flow visualization results for the blockage effect of the heated manikin.*

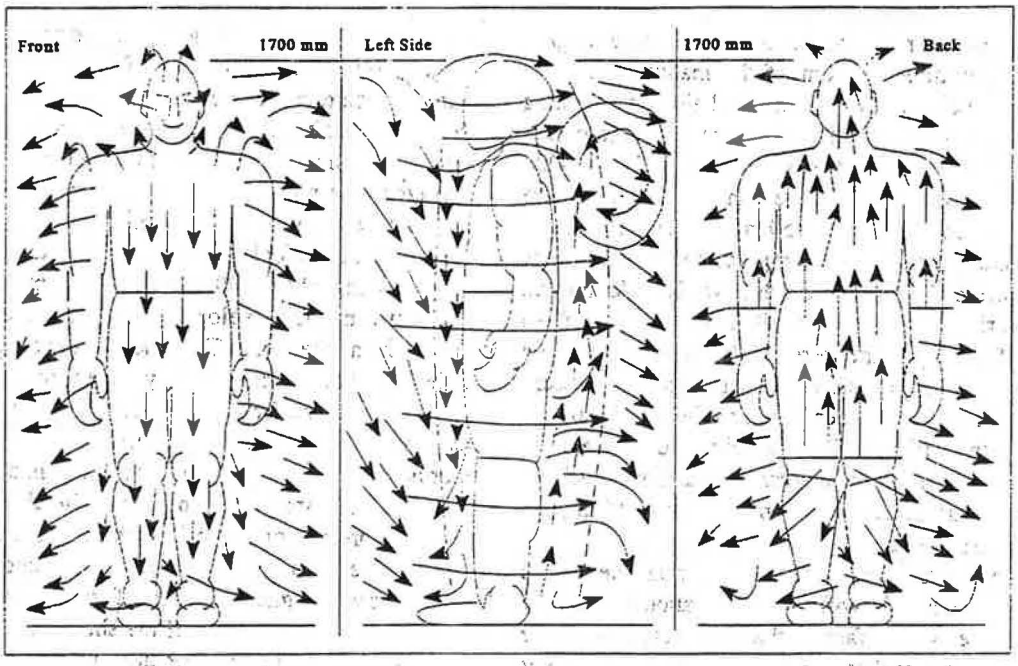

Figure 12 *Local airflow patterns near the thermal manikin for the mixed convection from the heated manikin.*

McCullough, E.A., and S. Hong. 1994. A data base for determining the decrease in clothing insulation due to body motion. *ASHRAE Transactions* 100(1): 765-775.

McCullough, E.A., B.W. Olesen, and S. Hong. 1994. Thermal insulation provided by chairs. *ASHRAE Transactions* 100(1): 795-802.

Miller P.L., and R.T. Nash. 1971. A further analysis of room air distribution performance. *ASHRAE Transactions* 77(2): 205-212.

Murakami, S.D., S. Kato, and Y. Suyama. 1988. Numerical and experimental study on turbulent diffusion fields in conventional flow type clean rooms. *ASHRAE Transactions* 94(1): 469-493.

Murakami, S., and S. Kato. 1989. Numerical and experimental study on room airflow—3-D predictions using the k-ε turbulence model. *Building and Environment*, 24(1): 85-97.

Myers, J.B. 1995. The interaction of room air movement and thermal plumes from the human body, *Master's thesis*, Kansas State University, Manhattan.

Rapp, G.M. 1973. Convective heat transfer and convective coefficients of nude man, cylinders and spheres at low air velocities. *ASHRAE Transactions* 79(1): 75-87.